Inelastic Neutron Scattering Spectra of Free Base and Zinc Porphines: A Comparison with DFT-Based Vibrational Analysis

Nina Verdal,[†] Pawel M. Kozlowski,[‡] and Bruce S. Hudson*[,†]

Department of Chemistry, Syracuse University, Syracuse, New York 13244, and Department of Chemistry, University of Louisville, Louisville, Kentucky 40292

Received: February 14, 2005; In Final Form: April 8, 2005

Inelastic neutron scattering (INS) spectra of free base (FBP) and zinc (ZnP) porphines are presented and compared with the results of density functional theory (DFT) calculations using the B3LYP functional with 6-31G(d) or 6-311G(d,p) basis sets. To obtain quantitative agreement between experiment and theory, two different scaling techniques have been applied: a scaled quantum mechanical (DFT-SQM) force field was developed for B3LYP/6-31G(d) calculations and the uniform frequency scaling technique (DFT-UFS) was applied to B3LYP/6-311G(d,p) results. The DFT-SQM calculations have been previously compared with IR and Raman spectra with good agreement, which allows for a nearly complete vibrational assignment. The results of the present study extend previous vibrational analysis to a higher level of reliability and complexity. The previous results are augmented by the comparison of calculated and observed INS intensities and the comparison of calculated modes with those observed in INS spectra but previously unobserved in optical spectra. Excellent agreement is acquired between the INS spectra and the results of both calculations, permitting a more detailed and reliable description of the vibrational properties of porphyrins.

Introduction

Free base porphine (FBP) is the simplest of all porphyrins, a group of molecules pervasive in biological systems.[1,2] A solid understanding of the structure and vibrations of the more complicated metalloporphyrins first requires a good understanding of the basic porphine macrocycle. FBP has two central hydrogen atoms on diametric pyrrole groups with an overall symmetry of D_{2h}. Removal of these hydrogen atoms as protons results in the D_{4h} dianion, which is the basic "core" unit for all biologically important porphyrins. This species strongly coordinates divalent cations such as Fe^{2+}, Zn^{2+}, Mg^{2+}, Ni^{2+}, etc. and may have a variety of peripheral substituents as well as axial ligands coordinated to the central metal. In iron-containing porphyrins, the central metal has multiple oxidation states, which is one of the main sources of the diversity of the biological function of heme-containing proteins. The biologically active iron porphyrins are often involved in oxidation/reduction reactions, which are controlled by small iron out-of-plane displacements. The modified "core" unit, i.e., a more saturated structure, is also present in other biological systems including chlorophyll, coenzyme B_{12} and cofactor F_{430}.

The nonfluorescent nature of iron porphyrins such as heme, combined with their wide distribution in nature at enzyme active sites, has made vibrational spectroscopies, in particular resonance Raman (RR) spectroscopy, of heme proteins widely used techniques in biophysical chemistry.[3] The RR spectroscopy relies on laser excitation resonant with one of the $\pi \rightarrow \pi^*$ electronic transitions, i.e., the Soret or Q-bands. Because both of these electronic transitions are in the porphine plane, only in-plane vibrations, primarily totally symmetric vibrations, are enhanced.

Initially, the detailed interpretation of such spectra relied on empirical correlations without theoretical treatments. Interpretation of RR spectra utilizes the frequencies of so-called "marker bands" associated with the geometry change of the porphyrin core as a consequence of a change in protein conformation, metal spin or oxidation state. The important step toward understanding metalloporphyrin vibrations was the development of an empirical force field (FF) pioneered by Gladkov and Solovyov,[4] Kitagawa,[5,6] and Spiro.[7,8] Kitagawa and co-workers were among the first to provide a theoretical background for the porphryin in-plane vibrations. The development of an empirical force field was further extended by Spiro and co-workers, but the majority of vibrational analysis has been restricted to in-plane vibrations only. Attempts have been made to extend this work to out-of-plane modes as well.[9] Due to the complexity and lack of reliable spectroscopic data, this is, however, a much more difficult task than for in-plane vibrations. Most of the empirical force field development has been guided by spectroscopic studies of nickel-containing porphyrins such as NiOEP (nickel octaethylporphyrin).[5,7,8] Nickel porphyrins have been used because they form stable four-coordinate complexes for which extensive vibrational data can be acquired including variable wave excitations and variety of isotopic substitutions. The development of the empirical force field for FBP has also been extended by Li and Zgierski.[10] This work took into account many spectroscopic data other than RR but, again, was restricted to the analysis of in-plane vibrations.

Vibrational analysis of porphyrins based on the application of ab initio methods as pioneered by Pulay (see for example refs 11 and 12 and references therein) has been hampered for a long time by the size and complexity of the porphyrin macrocycle. Early quantum mechanical calculations have shown that the structure of the FBP strongly depends on the level of theory and can lead either to a bond-localized structure with C_{2v} symmetry or a bond-equalized structure with D_{2h} symmetry. Available X-ray data, which is currently about 40 years old, by Webb and Fleischer[13,14] and Tulinsky[15] were not sufficiently

[†] Syracuse University.
[‡] University of Louisville.

10.1021/jp0507795 CCC: $30.25
Published on Web 06/04/2005

accurate to resolve this dilemma. Almlöf and co-workers[16] have demonstrated that a structure with localized double bonds is an artifact of calculations and the inclusion of correlation energy is critical for the correct treatment of this symmetry breaking problem. The important breakthrough came with the introduction of nonlocal density functional theory (DFT), which allows for the cost-effective analysis of structural and vibrational properties of complex systems such as metalloporphyrins. The application of DFT to FBP employing the B3LYP functional has demonstrated that this level of theory produces much more accurate results for essentially a fraction of computer time in comparison with other ab initio methods and the vibrational force field reproduces nearly accurately the essential vibrational properties of FBP.[17] The problem associated with symmetry breaking has been definitively resolved resulting in the correct prediction of the Kekule motion: the alternating expansion and contraction of the bonds along the conjugated ring.[18]

Quantum chemical calculations, including DFT, predict vibrational frequencies that are systematically overestimated. This overestimation is a consequence of insufficient treatment of the correlation energy, truncation of a basis set, or anharmonicity. Pulay and co-workers[19] recognized that such overestimation can be systematically corrected in a cost-effective way by the scaling of force constants. This procedure is commonly referred to as the scaled quantum mechanical (SQM) method and is considered to have higher precision than other techniques. The development of an SQM force field requires transformation of the Cartesian to internal force constants and the introduction of several scaling factors usually associated with distinct internal coordinates. To develop reliable scaling factors, a set of experimental frequencies is required for a least-squares fit to minimize the difference between experiment and theory.[20] Although vibrational analysis of FBP has been the subject of many experimental studies, it was the unique spectroscopic data in the form of matrix-isolated data published by Michl, Radziszewski, Waluk, and co-workers[21] that were key in previous DFT-based normal coordinate analysis. The combination of this unique spectroscopic data with DFT calculations resulted in the development of an essentially definitive force field. Nearly 500 vibrations (including isotopomers) were used to reproduce FBP vibrations with an accuracy below 5 cm^{-1}. Again, it should be pointed out that only a few out-of-plane vibrations were used to develop the DFT-SQM force field. The other frequently used approach in such studies is uniform frequency scaling (UFS). Only one scale factor is applied to all frequencies and overestimation is compensated by multiplication of each frequency by a number around 0.97. Generally, a much better quality basis set is required to obtain the same quality of results for DFT-UFS as for DFT-SQM.

Over the past few years the development of a DFT-SQM force field for FBP has been extended to other metallopoprhyrins including simple unsubstituted magnesium (MgP),[22] zinc (ZnP),[22] nickel (NiP),[23] and iron (FeP) porphines,[24] as well as metalloporphyrins with peripheral substituents including NiTPP[25] or NiOEP,[26] as well as iron porphyrins with axial ligands such as imidazole[27] or ligands including CO, O_2, or NO.[28,29] It can therefore be argued that a more complete understanding of the porphine vibrations can be accomplished with the availability of new experimental data, which will place application of DFT calculations on a firmer basis. In particular, inelastic neutron scattering (INS) provides coverage of a lower frequency region of the vibrational spectrum than is available in optical spectroscopies. Further, the ability to compute INS transition intensities provides a check on the interpretation of the entire vibrational spectrum.

The inelastic neutron spectra presented here provide strong support for the normal-mode frequencies and displacements calculated for FBP and ZnP. The inelastic neutron scattering spectra exhibit many vibrations that are not observed in optical spectra. Therefore, this study augments the optical spectroscopic experiments and provides a more complete picture of the normal modes of these molecules. In addition it provides a gauge for the quality of DFT-SQM and DFT-UFS calculations for molecules of this size.

Materials and Methods

Samples of approximately 1 g of FBP and ZnP (Frontier Scientific) were cooled to approximately 25 K for data collection at ISIS, the pulsed neutron source at Rutherford Appleton Laboratories. The inelastically scattered neutron spectrum was measured using the time-of-flight spectrometer TOSCA. TOSCA is able to collect spectra over a range of about 4−1000 meV (32−8000 cm^{-1}) with a resolution of 1.5−3.0% of the energy transfer ($\Delta\omega/\omega$).[30−32] The data presented were collected over the range 4−500 meV (32−4000 cm^{-1}). The backscattering spectra are chosen over the forward scattering spectra for presentation due to lower background levels and fewer effects from multiple scattering events.

Calculations

The geometries of FBP and ZnP were optimized under D_{2h} and D_{4h} symmetry constraints, respectively, followed by vibrational analysis. In all calculations the B3LYP[33,34] exchange-correlation functional was used with 6-31G(d) and 6-311G(d,p)[35,36] basis sets as implemented in the Gaussian 03 suite of programs for electronic structure calculations.[37] The Cartesian force constants computed at the B3LYP/6-31G(d) level of theory were transformed to natural internal coordinate systems[38] automatically generated by the SCALE program[39,40] and manually augmented. The resulting force constants were scaled according to

$$F'_{ij} = (\lambda_i \lambda_j) F_{ij} \quad (1)$$

where F_{ij} is the unscaled force constant and λ_i and λ_j are the scaling factors.[18] The 108 nonredundant coordinates of porphine were classified into internal coordinates that required a total of eight force field scaling factors. The initial values of scaling factors were obtained from a transferable set of parameters established from a set of 20 organic molecules and were further optimized by minimizing the weighted mean-square deviation between the calculated and the observed (by infrared absorption and Raman scattering) fundamental frequencies for FBP and five FBP isotopomers.[18,41] The 105 nonredundant coordinates of ZnP were classified into groups such that six of the force constant scaling factors optimized for FBP were used to calculate the frequencies for ZnP.[22] The difference in the number of scaling factors applied to FBP and ZnP comes from the hydrogens present inside the free base porphyrin core. Two additional factors were needed to obtain good agreement with experiment, whereas in the case of ZnP and other metalloporphyrins the same scaling factor was applied to describe the metal−nitrogen stretch and bending motion as was used for other atoms in the macrocycle.

The DFT-UFS calculations were performed using the B3LYP/6-311G(d,p) level of theory and applying one scaling factor obtained by direct comparison of the observed INS spectrum

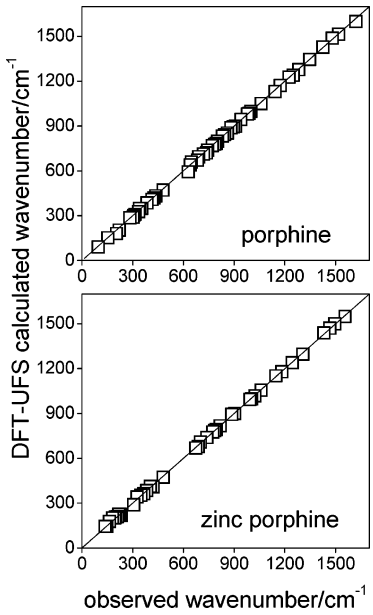

Figure 1. Correlation between the vibrations calculated with uniformly scaled density functional theory and the frequencies observed in the inelastic neutron scattering spectra.

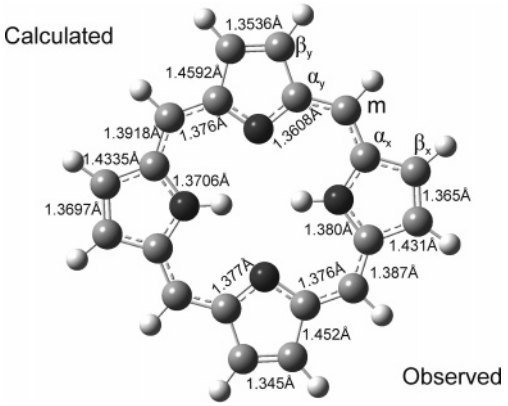

Figure 2. Free base porphine labeled with bond lengths calculated from a DFT B3LYP/6-311G(d,p) calculation and with symmetry-averaged bond lengths determined from room-temperature X-ray crystallography.[15]

with computed frequencies. The best agreement between calculated and observed frequencies occurs when the calculated frequencies of FBP are uniformly scaled by 0.975 and the calculated frequencies of ZnP are uniformly scaled by 0.979. A plot of the observed and uniformly scaled calculated vibrations is shown in Figure 1. Frequencies in the range 50−1600 cm^{-1} were included in this fit. Taking into consideration that CH vibrations in the 3000 cm^{-1} region are known to be characteristically anharmonic and the breadth and nature of inelastic neutron scattering spectra at this wavenumber results in diffuse features, these data were excluded from this analysis. The DFT-UFS technique can be viewed as a special case of the DFT-SQM method, which utilizes only one scaling factor in eq 1. In the case of the DFT-UFS approach, the transformation to internal coordinates is not necessary, but usually a much better quality basis set is required to compensate for the absence of multiple scaling factors.

Results

Molecular Geometry. Figure 2 represents the equilibrium geometry of FBP calculated using B3LYP/6-311G(d,p) assuming D_{2h} molecular symmetry. By convention[18,42] the nitrogen-bonded hydrogen atoms lie along the *x*-axis of porphine. The IUPAC recommendation for FBP is to label the plane of the molecule *yz* with the N−H bonds coinciding with the *z* direction. However, it is more convenient to label the plane as *xy* because it correlates directly with D_{4h} symmetry. The ZnP axes are assigned similarly with *x* and *y* in the plane of the molecule, and the *z*-axis out of the molecular plane. Figure 3 shows the equilibrium geometry of ZnP calculated using B3LYP/6-311G(d,p), with D_{4h} symmetry. The equilibrium geometry of both of these molecules is calculated to be planar. Tables 1 and 2 list the bond lengths for FBP and ZnP respectively, comparing the calculated values with the values determined from X-ray diffraction data.

Crystal structure analysis of free base porphine at room temperature[15] determined the molecule to be planar within ±0.02

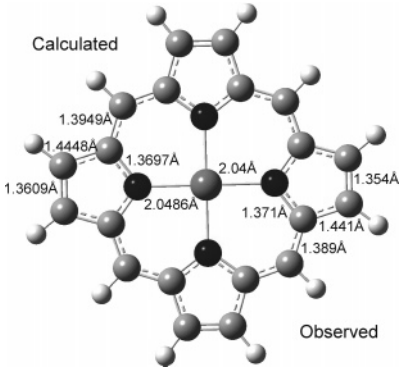

Figure 3. Zinc porphine labeled with bond lengths calculated from a DFT B3LYP/6-311G(d,p) calculation and with symmetry-averaged bond lengths determined from room-temperature X-ray crystallography of five distinct molecules in two distinct polymorphs.[43,44]

TABLE 1: Calculated and Observed[15] Bond Lengths of Free Base Porphine (Å)

	DFT		exp	std dev	Δ(cal − exp)	
R	6-31G(d)	6-311G(d,p)	(av)	(exp)[a]	6-31G(d)	6-311G(d,p)
α_xN	1.3727	1.3706	1.380	0.003	−0.007	−0.009
$\alpha_y\beta_y$	1.4600	1.4592	1.452	0.011	0.008	0.007
α_yN	1.3637	1.3608	1.377	0.012	−0.013	−0.016
α_ym	1.4003	1.3981	1.376	0.004	0.024	0.022
mα_x	1.3942	1.3918	1.387	0.008	0.007	0.005
$\alpha_x\beta_x$	1.4354	1.4335	1.431	0.006	0.004	0.002
$\beta_x\beta'_x$	1.3723	1.3697	1.365	0.008	0.007	0.005
$\beta_y\beta'_y$	1.3570	1.3536	1.345	0.001	0.012	0.009
$N_xN'_x$	4.2336	4.2271	4.112		0.122	0.115
$N_yN'_y$	4.0612	4.0621	4.056		0.005	0.006
N−H	1.0153	1.0134				
H···H	2.2029	2.2002				

[a] Standard deviation of the experimental values for the two ($\beta\beta'$ and NH) or four crystallographically inequivalent values that are symmetry related for the isolated molecule in D_{2h}.

TABLE 2: Calculated and Observed[43] Bond Lengths of Zinc Porphine (Å)

	DFT		exp	std dev	Δ(cal − exp)	
R	6-31G(d)	6-311G(d,p)	(av)	(exp)[a]	6-31G(d)	(6-311G(d,p))
αm	1.3956	1.3949	1.389	0.005	0.007	0.006
$\alpha\beta$	1.4454	1.4448	1.441	0.003	0.004	0.004
Nα	1.3734	1.3697	1.371	0.005	0.002	−0.001
Zn−N	2.0432	2.0486	2.04	0.01	0.0	0.01
$\beta\beta'$	1.3637	1.3609	1.354	0.003	0.010	0.007
N···N′	4.0863	4.0973	4.1	0.1	0.0	0.0

[a] Standard deviation of the experimental values for five crystallographically inequivalent molecules each with four (for $\beta\beta'$ and ZnN) or eight crystallographically inequivalent bond lengths that are symmetry related for the isolated molecule in D_{4h}.

Å. Standard deviations of the free base porphine bond lengths are estimated to be between 0.004 and 0.007 Å. The planar molecule exhibits C_{2h} symmetry and approximate D_{2h} symmetry. This is contradictory to those calculations that predict a bond-localized C_{2v} geometry corresponding to individual resonance forms and are noted to have insufficient electron correlation.[16] The stabilization reported[16] for the D_{2h} to C_{2v} deformation in an SCF calculation is only ca. 800 cm^{-1}. On the other hand, the fact that an approximate D_{2h} geometry is observed in the crystal does not preclude the possibility that a C_{2v} symmetry structure has the lowest energy and that both structures exist in the crystal. If these structures are randomly distributed or (equivalently to a diffraction study) interconverting, the resulting diffraction data will result in a higher symmetry structure. Despite the preferential D_{2h} symmetry of the isolated molecule, it is quite possible that, if low-energy deformation to a localized C_{2v} structure is possible, this would be stabilized in the crystal lattice because of the induction of an in-plane dipole moment.

In this respect it is surprising that FBP crystals form with a preferential orientation of the NH−HN (*x* axis) direction; i.e., interchanging the two protons of one molecule in the unit cell should result in a structure with very nearly the same energy. If this were the case, then diffraction analysis would show a D_{4h} structure with half-occupancy of the imino hydrogen atoms. This is what was reported in an earlier X-ray diffraction study.[13,14] Such a result is consistent with either static NH−HN disorder or dynamic interchange. Dynamic interchange of the imide protons in the crystalline state at room temperature is, in fact, indicated by ^{13}C and ^{15}N CP/MAS solid-state NMR studies.[45,46] This interpretation of the proton dynamics of crystalline porphine is inconsistent with the localized proton interpretation of the X-ray data in the most recent study. The most recent crystallographic study of FBP[15] was performed with special emphasis on the location of the internal imino N−H protons. The two adjacent pyrrole ring geometries are reported to differ significantly from one another, in support of specific N−H locations (see α and β bond lengths in Table 1). In this context it should be noted that the calculations for the isolated porphine molecule are in rather good agreement with the X-ray structure interpretation except for the internal N−H bond lengths, which were reported to be unreasonably short. This largely reflects the well-known[47,48] tendency of X-ray results toward short bond lengths due to the asymmetric location of the electrons relative to the hydrogen nucleus in X−H bonds. This is revealed in comparisons of X-ray and neutron structures that result in an apparent shortening of ca. 0.10−0.15 Å. The standard N−H bond length deduced from neutron scattering studies is 1.009 Å.[48] The calculated values are listed in Table 1. It should be noted that the H−H distance computed for FBP is slightly smaller than the sum of the standard van der Waals radii of 1.2 Å.

The reported crystal structure data for ZnP is an average of five crystallographically distinct molecules from two crystal structures[43,44] at room temperature. The bond lengths from each of those molecules were averaged under the assumption of D_{4h} molecular symmetry and a planar molecule. Because the reported data consist of an average of five structures, the deviation in observed bond lengths is greater than the experimental precision.

Tables 1 and 2 include bond lengths calculated using the B3LYP functional with two different basis sets. Comparison of the calculated bond lengths with the crystallographically determined bond lengths indicates that the results are not sensitive to basis set. Comparison of the last three columns of both tables shows that the difference between calculated and reported distances is of the same magnitude as the deviation in the experimentally determined, symmetry averaged, values. This indicates that the deformation due to the intermolecular interactions is roughly equivalent to the theory-experiment differences.

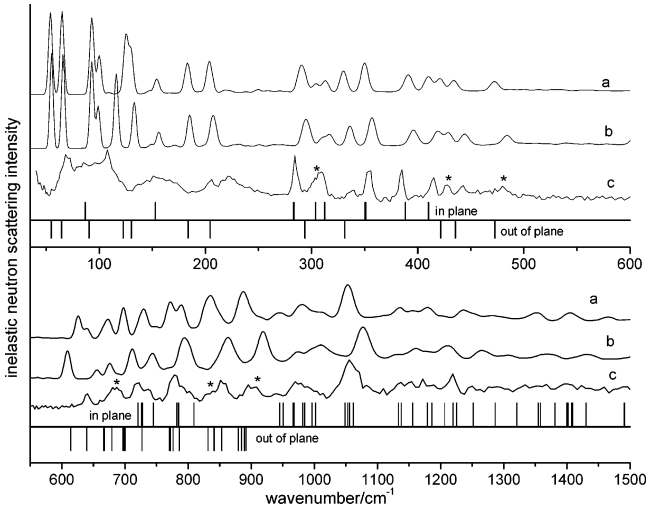

Figure 4. Free base porphine spectra. (a) DFT-SQM results, spectrum simulated with aClimax. (b) DFT-UFS results, spectrum simulated with aClimax. (c) Observed inelastic neutron scattering spectrum. The asterisks denote vibrations that have not been observed with optical spectroscopy. These are listed in Table 3. The sticks denote frequencies of vibrations calculated with DFT-SQM, with hydrogen motion in the molecular plane ("up") or out of the molecular plane ("down").

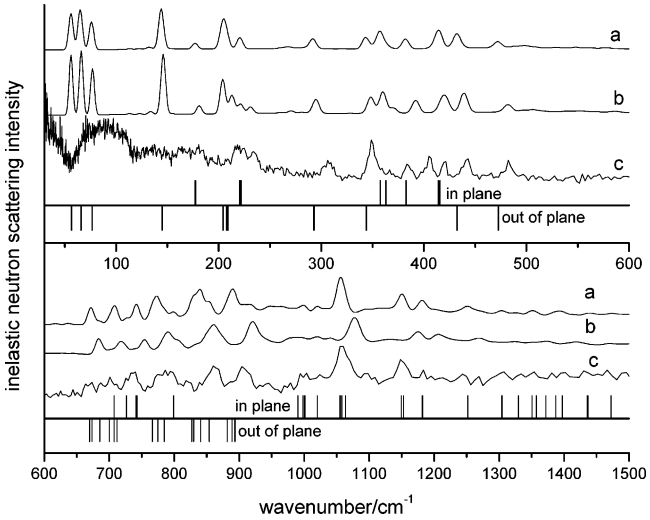

Figure 5. Zinc porphine spectra. (a) DFT-SQM results, spectrum simulated with aClimax. (b) DFT-UFS results, spectrum simulated with aClimax. (c) observed inelastic neutron scattering spectrum. These are listed in Table 3. The sticks denote frequencies of vibrations calculated with DFT-SQM, with hydrogen motion in the molecular plane ("up") or out of the molecular plane ("down").

Experimental and Simulated Spectra

Inelastic neutron scattering spectra of FBP and ZnP are shown in Figures 4 and 5. These graphs consist of the observed spectrum (lower trace) and spectra simulated by aClimax software[49] (two upper traces) employing the DFT-SQM and DFT-UFS frequency calculations. These spectra are scaled in magnitude and offset for ease of comparison. Both frequency calculations have been performed for a single molecule corresponding to optimized structures with bond lengths summarized in Figures 2 and 3. The solid state effects, which are particularly

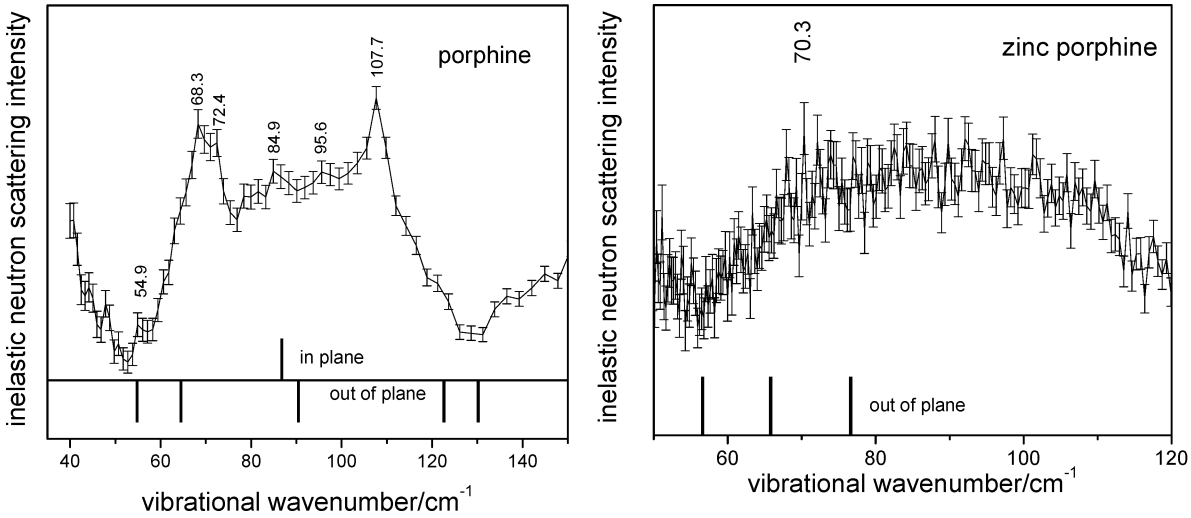

Figure 6. Low-frequency region of the inelastic neutron scattering spectra of porphine and zinc porphine are shown with DFT-SQM calculated frequencies shown as vertical lines and categorized as in plane or out of plane vibrations.

important for the low-frequency part of the INS spectrum, were not included in the computational analysis.

aClimax[49] uses the results from, in this case, a Gaussian[37] output file to calculate the relative intensities of molecular fundamental, combination and overtone transitions in addition to phonon sidebands. An efficient way to do this is to use a low-frequency region of the observed spectrum that is assumed to be composed primarily of fundamental phonon transitions and use it to simulate a phonon density of states. The phonon frequency range can be adjusted as required, as can the relative intensities of the phonon sideband to the molecular fundamentals. Additionally, the aClimax simulation is optimized for agreement with the observed spectral line width for the TOSCA spectrometer.

The intensity of an observed INS transition is determined by the square of the hydrogen displacement upon vibrational excitation, weighted by the inelastic neutron scattering cross section and a Debye−Waller factor. The relative intensities of the calculated inelastic scattering peaks are roughly in good agreement with the relative intensities of the observed peaks. This is an indication that the calculated normal mode eigenvectors that involve hydrogen motion approach a correct description of the molecular vibrations. In general, the similarities between the two calculations are greater than the similarities between one calculation and the observed spectrum. This indicates that either method will predict the vibrational eigenvectors with similar accuracy.

Although minor, there are differences between the relative intensities of the DFT-SQM calculation and the DFT-UFS calculation. These are most noticeable at lower vibrational frequencies. In this region the DFT-UFS method predicts a larger relative intensity (i.e., greater hydrogen displacement) in the low-frequency modes than does the DFT-SQM method. It is worth noting that these computed spectra are based on an isolated molecule model, whereas much of what is observed in this low-frequency region results from the collective motions of molecules in a crystal.

The relative intensities in the FBP spectra within the range 100−500 cm^{-1} calculated using DFT-UFS appear to be in better agreement with experiment than the DFT-SQM calculated relative intensities. However, within the range 750−1100 cm^{-1} the SQM results seem to be in better agreement with the observed relative peak intensities. Neither calculation is perfect in reproducing the 600−750 cm^{-1} region in which it appears the relative frequencies of overlapping peaks is important in the gauging the accuracy of the relative intensities.

In the ZnP case, the DFT-UFS calculation results are in better agreement with the experiment than the DFT-SQM results in the 1240−1615 cm^{-1} range of the spectra. The DFT-SQM method appears to better reproduce experimental relative intensities in the 300−485 cm^{-1} range. Both calculations seem to be in equal agreement with the observed relative intensities in the 650−1182 cm^{-1} range. Neither method predicts the 0−300 cm^{-1} spectral region with much accuracy, but again, this is a region dominated by phonons, compared with the results of a single molecule calculation. The DFT-SQM method, however, better predicts the intensities of the peaks in this area relative to the intensities of the peaks at higher frequencies. The differences between the two calculation results are probably not directly due to the method of frequency scaling but most likely reflect a difference in the quality of basis sets used in these calculations.

Low-Frequency Region. The low-frequency regions observed in the inelastic neutron scattering spectra are shown in Figure 6. In these spectra, as with many crystalline systems, the lowest frequency vibrations overlap with the broad phonon band. In the ZnP spectrum the signal-to-noise ratio is only good enough to imagine a vibrational transition at about 70 cm^{-1} that could be assigned to the b_{1u} mode calculated to be 65.8 cm^{-1} in DFT-SQM or 65.2 cm^{-1} in DFT-UFS. It could also be assigned to the doming mode of a_{2u} symmetry calculated at 76.6 cm^{-1} (DFT-SQM) and 75.6 cm^{-1} (DFT-UFS). Neither mode has been observed in optical spectroscopy.

In the FBP INS low-frequency spectrum there are some resolved peaks atop a broad phonon band (Figure 6). At the very edge of the broad band is a shoulder at 55 cm^{-1} that may be attributed to the saddle mode calculated at 54.8 cm^{-1} (DFT-SQM) or 54.1 cm^{-1} (DFT-UFS) with b_{1u} symmetry. The doming mode is calculated at 90.5 cm^{-1} (DFT-SQM) or 91.6 cm^{-1} (DFT-UFS) with b_{1u} symmetry and could be paired with either the transition observed at 85 cm^{-1} or the one observed at 96 cm^{-1}. The transition observed at 68.3 cm^{-1} or that observed at 72 cm^{-1} could be assigned the a_u mode calculated at 64.5 cm^{-1} (DFT-SQM) or 64.5 cm^{-1} (DFT-UFS). The relatively intense mode observed at 108 cm^{-1} can be assigned to the b_{1g} mode calculated at 86.8 cm^{-1} (DFT-SQM) or 97.5 cm^{-1} (DFT-UFS),

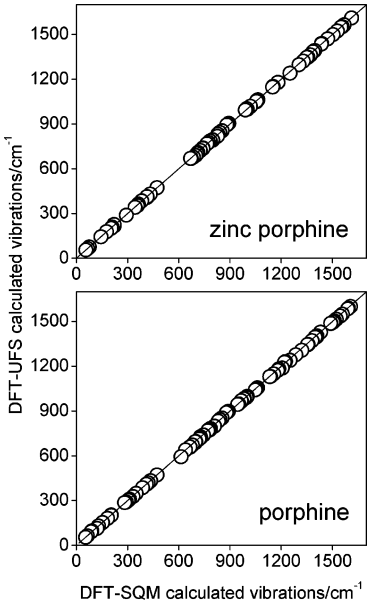

Figure 7. DFT-UFS calculated vibrations vs DFT-SQM calculated vibrations. If the two calculations gave identical results, points would fall on the solid $y = x$ line.

confirmed by previous observation in resonance Raman spectra.[41]

Analysis of Molecular Vibrations. The vibrational frequencies calculated using the DFT-SQM method are plotted against those calculated using the DFT-UFS method and compared with a solid $y = x$ line as shown in Figure 7. These calculated values are in close agreement with one another and with the observed inelastic neutron scattering data. The average difference between (54) INS observed frequencies and DFT-SQM calculated frequencies for free base porphine is 8 cm^{-1}; the average difference between observed and DFT-UFS calculated frequencies with a scale factor of 0.975 is 11 cm^{-1}. The agreement between zinc porphyrin INS observed and calculated frequencies is even better than that for free base porphine, probably due to the higher symmetry of the zinc porphine. The average difference between (40) observed and DFT-SQM calculated zinc porphine frequencies is 6 cm^{-1}. The average difference between INS observed and DFT-UFS calculated frequencies, using a scale factor of 0.979, is also 6 cm^{-1}. Based on the quality of the linear fit to the data, the DFT-SQM method predicts zinc porphine vibrational frequencies with the same accuracy as the uniformly scaled DFT. In the case of free base porphine, the DFT-SQM method is a slightly better predictor of frequencies than the uniformly scaled DFT results.

Tables S1 and S2 in the Supporting Information compare observed and calculated frequencies of FBP and ZnP. The tables list frequencies calculated by DFT-SQM (B3LYP/6-31G(d)) and DFT-UFS (B3LYP/6-311G(d,p)). The observed inelastic neutron scattering vibrational frequencies are listed in addition to previously published values of frequencies observed with optical spectroscopy methods.[18,22,41] Due to the decreased resolution in the inelastic neutron scattering spectra and due to an increasing number of multiphonon and multiquanta transitions, the uncertainty in the assignment of observed transitions increases as energy transfer increases. Peak frequencies with a greater uncertainty due either to overlapping peaks or to decreased instrument resolution are listed in parentheses in tables S1 and S2. At vibrational wavenumbers of less than 1500 cm^{-1}, the inelastic neutron scattering spectra are sufficiently well resolved to demonstrate the presence of vibrational transitions that are not observed in optical spectroscopies such as infrared absorption or Raman scattering.

A demonstration of the number of vibrations observed in INS spectroscopy relative to the number observed in infrared absorption, Raman scattering, or fluorescence is shown in Figure 8 for FBP and Figure 9 for ZnP. It is clear from these figures that INS provides more data for comparison with calculated results than those spectroscopies with vibrational symmetry restrictions. A list of the frequencies observed in INS spectroscopy, predicted in DFT-SQM calculations, and not previously

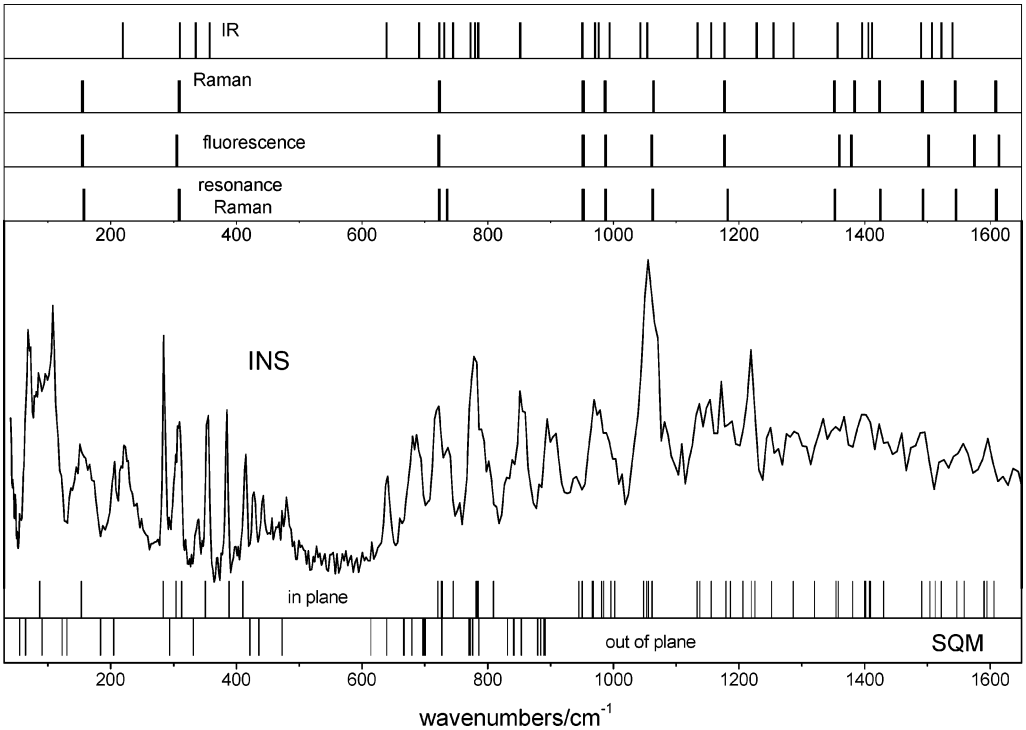

Figure 8. Observed and DFT-SQM calculated vibrations for free base porphine. See ref 41 for nonresonant Raman data, also ref 50 for matrix isolated fluorescence data, and refs 4, 51, and 52 for resonance Raman data.

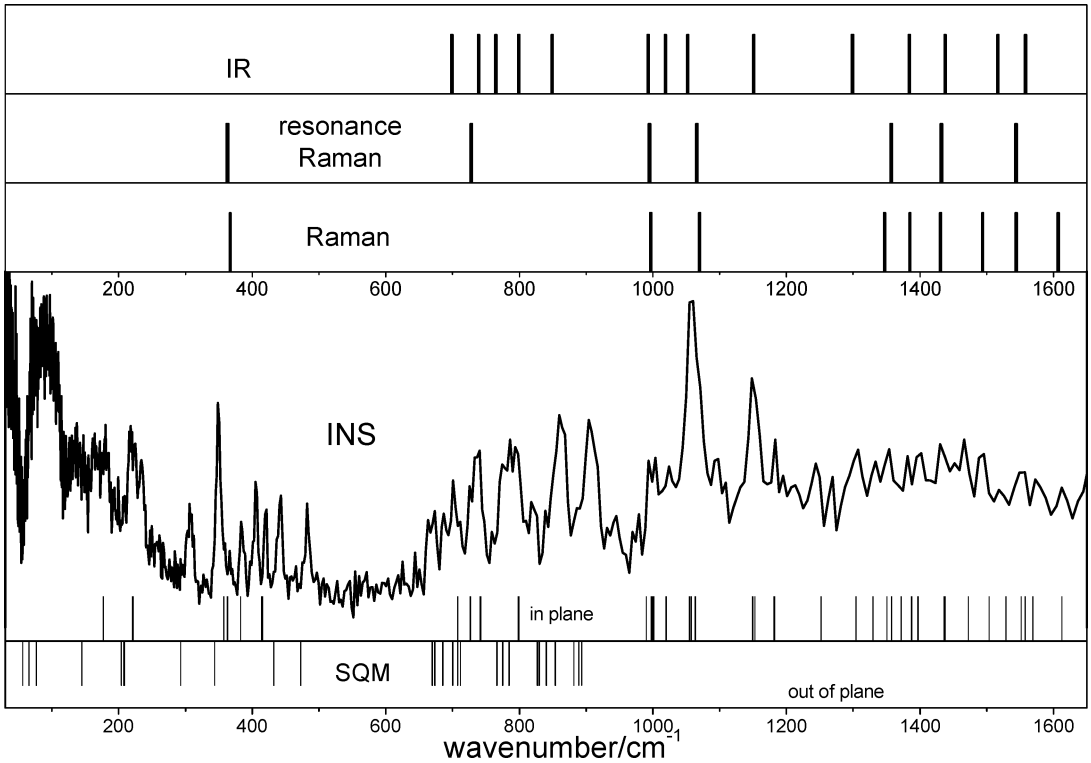

Figure 9. Observed and DFT-SQM calculated vibrations of zinc porphine. For IR, Raman and resonance Raman data see ref 22.

TABLE 3: Vibrations That Have Not Been Observed in Optical Spectroscopy but Have Been Observed in INS[a]

Free Base Porphine

obs (cm^{-1})	calc (cm^{-1})	symmetry (D_{2h})
55	54.8	b_{1u}
68	64.5	a_u
303	293.7	a_u
426	421.5	b_{2g}
480	472.7	a_u
684	679.5	a_u
831	831.7	a_u
908	891.7	a_u

Zinc Porphine

obs (cm^{-1})	calc (cm^{-1})	symmetry (D_{4h})
482	472.5	b_{1u}
674	673.5	e_g
687	685.4	a_{1u}
774	775	e_g
786	784.6	b_{2u}
818	827	b_{2g}
886	881.7	a_{1u}
1060	1057.8	b_{1g}
1183	1182.4	b_{1g}
1244	1251.9	e_u
1466	1472.4	b_{2g}

[a] The observed vibrations are compared with SQM-calculated frequencies.

observed in optical spectroscopies, is presented in Table 3. Of course, the advantage of symmetry-restricted spectroscopy is that mode assignment is more direct than in INS. In this respect, the use of a combination of spectroscopic techniques can be very powerful. Full listings of the proposed assignments for the isolated free base porphine molecule and the zinc porphine molecule are found in Tables 4 and 5. The calculated vibrations are compared with the vibrations observed in condensed phase spectroscopy. Small discrepancies between calculated and spectroscopically observed frequencies may be attributed to matrix-imposed forces on the molecule.

Conclusions

Vibrational transitions have been observed with inelastic neutron scattering that are not observed with optical spectroscopies. This augments the optical data and provides a more extensive gauge for the accuracy of both the scaled quantum mechanical and density functional methods. The large number of observed fundamental vibrations in the inelastic neutron scattering spectra relative to Raman, infrared, resonance Raman, and matrix-isolated fluorescence spectra emphasizes that it is an ideal spectroscopic technique (although favorably augmented by optical spectroscopies) for comparison with the low-frequency results ($\sim$100$-$1500 cm^{-1}) of a ground-state normal mode calculation.

The two DFT calculations presented here produce results of roughly the same quality. The differences between SQM (using B3LYP/6-31G(d)) calculated and INS observed frequencies are less than or comparable to the differences between uniformly scaled DFT (using B3LYP/6-311G(d,p)) and INS observed frequencies. The frequencies and relative intensities observed in the neutron scattering spectra are reproduced with reasonable accuracy by these calculations. Not only do the calculated frequencies agree well with the vibrational frequencies observed in inelastic neutron scattering spectra but they also show good agreement with frequencies observed with optical spectroscopies such as matrix isolated fluorescence, infrared absorption, and Raman scattering.

The spectral simulation is based on an isolated molecule model. This simple model appears to be validated by the level of agreement with the vibrational data and INS intensities to a degree that is on the order of expectations based on other cases.[53−56] The model and the underlying computational method are also validated by the extent of agreement with the observed molecular structures based on the X-ray study. Together these two comparisons indicate that the interpretation of the X-ray diffraction study, in which the imino hydrogens are localized, is correct. In particular, the distinct geometries of the "*x*" and

TABLE 4: Vibrational Assignment of Free Base Porphine[a]

mode		calc	obs	mode	calc	obs
		a_g Symmetry			a_u Symmetry	
1	ν_{NH}	3366.2		55	891.7	**908, 895**
2	ν_5	3123.8	**3146**	56	879.7	**(882)**
3	ν_{14}	3109.1		57	831.7	**(831)**
4	ν_1	3058.9		58	698.5	**691**
5	ν_{10}	1605.9	1609, 1610, 1614	59	679.5	**684**
6	ν_2	1558.7	1544, 1546, 1575	60	472.7	**480**
7	ν_{11}	1504.2	1492, 1493, 1502	61	293.7	**303**
8	ν_3	1430.4	1424, 1425	62	64.5	**70, 72**
9	ν_4	1402.0	1384			
10	ν_{12}	1358.1	1352, 1353, 1360		b_{1u} Symmetry	
11	ν_{13}	1179.3	1177, 1182	63	853.3	852
12	ν_9	1061.9	1061, 1063, 1064	64	786.0	785
13	ν_{17}	1055.8	1061, 1063	65	776.1	773
14	ν_6	984.7	987, 988	66	727.1	731
15	ν_{15}	950.8	952	67	696.7	691
16	ν_7	727.8	736	68	639.4	639
17	ν_{16}	720.6	722, 723	69	331.3	335
18	ν_8	303.8	309, 305	70	204.5	219
19	ν_{18}	152.9	155, 157	71	90.5	**87, 94, 96**
				72	54.8	
		b_{1g} Symmetry				
20	ν_{23}	3107.3	3109		b_{2u} Symmetry	
21	ν_{31}	3088.8	**(3083)**	73	3109.0	3124
22	ν_{27}	3058.8	**3007**	74	3107.3	3112
23	ν_{19}	1590.3	1600, 1578	75	3058.8	3045
24	ν_{28}	1491.2	1493, 1497	76	1594.6	
25	ν_{20}	1381.1	1400, 1388	77	1546.8	1540
26	ν_{29}	1354.7	1350, 1352, 1374	78	1490.9	1490
27	ν_{26}	1320.5	1313, 1318, 1316	79	1409.3	1406
28	δ_{NH}	1219.5	1226, 1221	80	1354.8	1357
29	ν_{34}	1186.3	1177, 1182	81	1251.7	1255
30	ν_{21}	1133.2	1138, 1134	82	1225.4	1228
31	ν_{30}	1002.1	1005, 1001	83	1155.8	1156
32	ν_{22}	966.5	976, 972	84	1053.0	1054
33	ν_{24}	809.4	805	85	981.5	977
34	ν_{32}	783.7	786	86	945.2	951
35	ν_{33}	410.2	418	87	781.6	
36	ν_{25}	388.4	389	88	745.2	745
37	ν_{35}	86.8	109	89	350.8	357
				90	283.3	**282, 284**
		b_{2g} Symmetry				
38		884.7	**(882)**		b_{3u} Symmetry	
39		841.7	**(843)**	91	3329.8	3324
40		772.2	**771**	92	3123.7	3128
41		700.3	**691**	93	3088.8	3088
42		667.2		94	3058.8	3042
43		614.1	**(628)**	95	1522.3	1522
44		421.5	**415, 426**	96	1512.2	1507
45		183.7	**166, 200, (204)**	97	1407.6	1412
46		122.6		98	1399.9	1396
				99	1286.3	1287
		b_{3g} Symmetry		100	1206.4	1177
47		889.3	**895**	101	1137.8	1134
48		841.0	**(843)**	102	1048.6	1043
49		770.3	**771**	103	996.3	994
50		700.3	**691**	104	968.0	971
51		666.1	**647**	105	785.1	780
52		435.5	**426, (436)**	106	726.2	723
53		204.5	**200, (204)**	107	350.3	357
54		130.2	**145**	108	312.4	310

[a] The normal mode symmetries and labels are derived from D_{2h} symmetry using standard conventions. The computed frequencies are from the DFT-SQM treatment for the isolated molecule. The condensed phase experimental values are from optical measurements, if available, due to their higher resolution. The details of this aspect of the assignment are presented in the Supporting Information, Table S1. The values given in bold are from the INS spectrum of this work. In some cases these values are in parentheses to indicate that the INS spectrum has overlapped peaks in this region. Frequencies are presented in wavenumber (cm^{-1}). The mode numbering in the first column follows the standard Mulliken system. The mode numbering in the second column is as used in ref 41.

"*y*" pyrrole rings are in agreement with the computed and X-ray structure in both sign and magnitude. The three distinct bond lengths of the pyrrole pairs (in D_{2h}) are reported to differ from each other by amounts whose root-mean-square (rms) deviation is 0.029 Å. These three numbers are themselves averages of two determinations each due to the low site symmetry. The magnitude of the difference between the "*x*" and "*y*" pyrrole groups is considerably larger than typical X-ray uncertainties for heavy atom bond distances. The calculated bond lengths differ in the same fashion by a similar amount (see Table 1) with an rms deviation of 0.032 Å. The linear correlation coefficient of the three calculated and observed differences is 0.92. The slope of the correlation is 0.88; i.e., the calculated

TABLE 5: Vibrational Assignment of Zn Porphine[a]

mode	calc	obs	mode	calc	obs
	a_{1g} Symmetry			a_{1u} Symmetry	
1	3114.1		44	881.7	**886**
2	3058.1		45	685.4	**687**
3	1557.7	1544	46	292.9	**284, 306**
4	1437.3	**1430**			
5	1371.8	1357			
6	1063.4	1066		a_{2u} Symmetry	
7	1001.4	996	47	854.1	849
8	726.6	728	48	766.3	765
9	363.0	367	49	711.9	700
			50	343.9	**327**
	a_{2g} Symmetry		51	209.0	**209**
10	3094.9		52	76.6	
11	1569.0	**(1557)**			
12	1350.6			b_{1u} Symmetry	
13	1329.6		53	893.5	**904**
14	1149.4	**1148**	54	829.8	**818**
15	1000.0	**1004**	55	700.3	**701**
16	798.8	**794**	56	472.5	**482**
17	415.7	**421**	57	65.8	
	b_{1g} Symmetry			b_{2u} Symmetry	
18	3113.6		58	784.6	**786**
19	1612.6	1607	59	669.6	**674**
20	1503.6	1494	60	207.7	**199**
21	1387.3	1385	61	56.6	
22	1182.4	**1183**			
23	1057.8	**1060**		e_u Symmetry	
24	997.9	997	62	3113.8	
25	741.7	**740**	63	3095.0	
26	177.2	**164**	64	3058.0	
			65	1551.5	1558
	b_{2g} Symmetry		66	1528.6	1517
27	3095.2		67	1436.0	1438
28	3057.9		68	1397.0	1384
29	1472.4	**(1466)**	69	1304.3	1299
30	1357.3	**1357**	70	1251.9	**1244**
31	1181.7	**1183**	71	1152.9	1152
32	1055.3	**1060**	72	1054.8	1052
33	827.0	**818**	73	1020.0	1019
34	414.2	**405**	74	990.2	993
35	221.8	234	75	799.2	799
			76	742.4	739
	e_g Symmetry		77	382.7	
36	775.0	**774**	78	357.5	
37	775.0	**774**	79	220.5	
38	707.6	**701**			
39	707.6	**701**			
40	673.5	**674**			
41	432.4	**421**			
42	144.9	**147**			
43	144.9	**137**			

[a] The normal mode symmetries and labels are derived from D_{4h} symmetry using standard conventions. The computed frequencies are from the DFT-SQM treatment for the isolated molecule. The condensed phase experimental values are from optical measurements, if available, due to their higher resolution. The details of this aspect of the assignment are presented in the Supporting Information, Table S2. The values given in bold are from the INS spectrum of this work. In some cases these values are in parentheses to indicate that the INS spectrum has overlapped peaks in this region. Frequencies are presented in wavenumber (cm^{-1}).

differences are slightly larger than the observed values. However, if the interpretation of the ^{13}C and ^{15}N NMR results that the protons rapidly exchange at room temperature is correct, then the expected crystal structure would appear to have molecular D_{4h} symmetry with no difference between the pyrrole bond lengths reflecting the *average* atomic positions. If this explanation were correct for all porphine crystals, then the degree of agreement between the structure observed by X-ray diffraction and that computed would have to be considered fortuitous.

A likely explanation is that porphine is polymorphic. The above crystal disorder issue is not relevant to the interpretation of the vibrational spectrum of porphine and does not arise for the case of zinc porphine. The use of an isolated molecule model for comparison with results obtained for the solid means that differences between the calculated and observed spectra may be due to intermolecular interactions. A summary of the assignments for all of the modes of free base and zinc porphine are given in Tables 4 and 5, respectively. For free base porphine the full listing of "optical" (IR, Raman, resonance Raman, or fluorescence) values is given. Both systematic and porphine-specific mode numbering schemes are given. For zinc porphine a particular optical value is chosen when several are available. In each case INS values are given when optical values are unavailable and these are shown in bold. The details of the data sources are given in the Supporting Information.

Previous work left open some questions of assignments. This included the a_g modes of free base porphine designated 6 (ν_2) and 9 (ν_4) in Table 4 where there are relatively large differences either between the calculated and observed frequencies or within the reported experimental values. Examination of this region of the INS spectrum and comparison with the computed spectrum showed that most of the intensity in this region is due to overtones and combinations. Because of this we cannot add to this issue with the available INS data. It is possible that momentum resolved spectra could sort out the contributions from fundamental transitions in this region. These tables reveal the remaining vibrations of these simple porphine systems for which there is at present no existing data.

Acknowledgment. We thank the Rutherford Appleton Laboratory for neutron beam access at the ISIS Facility, where the TOSCA spectrometer was used, in addition to the TOSCA staff for their assistance. This work was supported by U.S. National Science Foundation grant CHE 0240104 and by the U.S. Department of Energy grant DE-FG02-01ER14245. The porphine and zinc porphine samples were rented from Frontier Scientific of Logan, UT. We thank Dr. John Shelnutt of Sandia National Laboratory for providing some details of the unpublished structure of zinc porphine.

Supporting Information Available: Tables S1 and S2 compare observed and calculated frequencies of FBP and ZnP. This material is available free of charge via the Internet at http://pubs.acs.org.

References and Notes

(1) *The Porphyrins*; Dolphin, D., Ed.; Academic Press: New York, 1978/1979; Vols. 1−7.

(2) *The Porphyrin Handbook*; Kadish, K. M.; Smith, K. M.; Guilard, R., Eds.; Academic Press: New York, 1999; Vols. 1−10.

(3) *Biological Applications of Raman Spectroscopy*; Spiro, T. G., Ed.; Wiley-VCH: New York, 1987.

(4) Solovyov, K. N.; Gladkov, L. L.; Gradyushko, A. T.; Ksenofontova, N. M.; Shulga, A. M.; Starukhin, A. S. *J. Mol. Struct.* **1978**, *45*, 267−305.

(5) Kitagawa, T.; Abe, M.; Oghoshi, H. *J. Chem. Phys.* **1978**, *69*, 4516−4525.

(6) Abe, M.; Kitagawa, T.; Kyogoku, Y. *J. Chem. Phys.* **1978**, *69*, 4526−4534.

(7) Li, X.-Y.; Czernuszewicz, R. S.; Kincaid, J. R.; Stein, P.; Spiro, T. G. *J. Phys. Chem.* **1990**, *94*, 47−61.

(8) Li, X.-Y.; Czernuszewicz, R. S.; Kincaid, J. R.; Su, Y. O.; Spiro, T. G. *J. Phys. Chem.* **1990**, *94*, 31−47.

(9) Li, X.-Y.; Czernuszewicz, R. S.; Kincaid, J. R.; Spiro, T. G. *J. Am. Chem. Soc.* **1989**, *111*, 7012−7023.

(10) Li, X.-Y.; Zgierski, M. Z. *J. Phys. Chem.* **1991**, *95*, 4268−4287.

(11) Fogarasi, G.; Pulay, P. *Annu. Rev. Phys. Chem.* **1984**, *35*, 191−213.

(12) Pulay, P. *J. Mol. Struct.* **1995**, *347*, 293−308.

(13) Webb, L. E.; Fleischer, E. B. *J. Am. Chem. Soc.* **1965**, *87*, 667−669.

(14) Webb, L. E.; Fleischer, E. B. *J. Chem. Phys.* **1965**, *43*, 3100−3111.

(15) Tulinsky, A.; Chen, B. M. L. *J. Am. Chem. Soc.* **1972**, *94*, 4144−4151.

(16) Almlof, J.; Fischer, T. H.; Gassman, P. G.; Ghosh, A.; Haser, M. *J. Phys. Chem.* **1993**, *97*, 10964−10970.

(17) Kozlowski, P. M.; Zgierski, M. Z.; Pulay, P. *Chem Phys Lett.* **1995**, *247*, 379−385.

(18) Kozlowski, P. M.; Jarzecki, A. A.; Pulay, P. *J. Phys. Chem.* **1996**, *100*, 7007−7013.

(19) Pulay, P.; Fogarasi, G.; Pongor, G.; Boggs, J. E.; Varga, A. *J. Am. Chem. Soc.* **1983**, *105*, 7037−7047.

(20) Rauhut, G.; Pulay, P. *J. Phys. Chem.* **1995**, *99*, 3093−3100.

(21) Radziszewski, J. G.; Waluk, J.; Neptras, M.; Michl, J. *J. Phys. Chem* **1991**, *95*, 1963−1969.

(22) Jarzecki, A. A.; Kozlowski, P. M.; Pulay, P.; Ye, B.-H.; Li, X.-Y. *Spectrochem. Acta Part A* **1997**, *53*, 1195−1209.

(23) Kozlowski, P. M.; Rush, T. S., III; Jarsecki, A. A.; Zgierski, M. Z.; Chase, B.; Piffat, C.; Ye, B.-H.; Li, X.-Y.; Pulay, P.; Spiro, T. G. *J. Phys. Chem. A* **1999**, *103*, 1357−1366.

(24) Kozlowski, P. M.; Spiro, T. G.; Berces, A.; Zgierski, M. Z. *J. Phys. Chem. B* **1998**, *102*, 2603−2608.

(25) Rush, T. S., III; Kozlowski, P. M.; Piffat, C.; Zgierski, M. Z.; Spiro, T. G. *J. Phys. Chem. B* **2000**, *104*, 5020−5034.

(26) Stoll, L. K.; Zgierski, M. Z.; Kozlowski, P. M. *J. Phys. Chem. A* **2003**, *107*, 4165−4171.

(27) Kozlowski, P. M.; Zgierski, M. Z.; Spiro, T. G. *J. Phys. Chem. B* **1999**, *104*, 10659−10666.

(28) Vogel, K. M.; Kozlowski, P. M.; Zgierski, M. Z.; Spiro, T. G. *J. Am. Chem. Soc.* **1999**, *121*, 9915−9921.

(29) Spiro, T. G.; Zgierski, M. Z.; Kozlowski, P. M. *Coord. Chem. Rev.* **2001**, *219−221*, 923−936.

(30) Bowden, Z. A.; Celli, M.; Cilloco, F.; Colognesi, D.; Newport, R. J.; Parker, S. F.; Ricci, F. P.; Rossi-Albertini, V.; Sacchetti, F.; Tomkinson, J.; Zoppi, M. *Physica B* **2000**, *276−278*, 98−99.

(31) Parker, S. F.; Carlile, C. J.; Pike, T.; Tomkinson, J.; Newport, R. J.; Andreani, C.; Ricci, F. P.; Sacchetti, F.; Zoppi, M. *Physica B* **1998**, *241−243*, 154−156.

(32) TOSCA. http://www.isis.rl.ac.uk/molecularspectroscopy/tosca/.

(33) Becke, A. D. *J. Chem. Phys.* **1993**, *98*, 5648.

(34) Lee, C.; Yang, W.; Parr, R. G. *Phys. Rev. B* **1988**, *41*, 785.

(35) Hehre, W. J.; Ditchfield, R.; Pople, J. A. *J. Chem. Phys.* **1972**, *56*, 2257−2261.

(36) Krishnan, R.; Binkley, J. S.; Seeger, R.; Pople, J. A. *J. Chem. Phys.* **1980**, *72*, 650−654.

(37) Frisch, M. J.; Trucks, G. W.; Schlegel, H. B.; Scuseria, G. E.; Robb, M. A.; Cheeseman, J. R.; J. A. Montgomery, J.; Vreven, T.; Kudin, K. N.; Burant, J. C.; Millam, J. M.; Iyengar, S. S.; Tomasi, J.; Barone, V.; Mennucci, B.; Cossi, M.; Scalmani, G.; Rega, N.; Petersson, G. A.; Nakatsuji, H.; Hada, M.; Ehara, M.; Toyota, K.; Fukuda, R.; Hasegawa, J.; Ishida, M.; Nakajima, T.; Honda, Y.; Kitao, O.; Nakai, H.; Klene, M.; Li, X.; Knox, J. E.; Hratchian, H. P.; Cross, J. B.; Adamo, C.; Jaramillo, J.; Gomperts, R.; Stratmann, R. E.; Yazyev, O.; Austin, A. J.; Cammi, R.; Pomelli, C.; Ochterski, J. W.; Ayala, P. Y.; Morokuma, K.; Voth, G. A.; Salvador, P.; Dannenberg, J. J.; Zakrzewski, V. G.; Dapprich, S.; Daniels, A. D.; Strain, M. C.; Farkas, O.; Malick, D. K.; Rabuck, A. D.; Raghavachari, K.; Foresman, J. B.; Ortiz, J. V.; Cui, Q.; Baboul, A. G.; Clifford, S.; Cioslowski, J.; Stefanov, B. B.; Liu, G.; Liashenko, A.; Piskorz, P.; Komaromi, I.; Martin, R. L.; Fox, D. J.; Keith, T.; Al-Laham, M. A.; Peng, C. Y.; Nanayakkara, A.; Challacombe, M.; Gill, P. M. W.; Johnson, B.; Chen, W.; Wong, M. W.; Gonzalez, C.; Pople, J. A. *Gaussian 03*, revision B.05 ed.; Gaussian, Inc.: Pittsburgh, PA, 2003.

(38) Fogarasi, G.; Zhou, X.; Taylor, P. W.; Pulay, P. *J. Am. Chem. Soc.* **1992**, *114*, 8191−8201.

(39) Pulay, P. TX90 Fayetteville, AR, 1990.

(40) Pulay, P. *Theor. Chim. Acta* **1979**, *50*, 299.

(41) Kozlowski, P. M.; Jarzecki, A. A.; Pulay, P.; Li, X.-Y.; Zgierski, M. Z. *J. Phys. Chem.* **1996**, *100*, 13985−13992.

(42) Note: Interchanging the *x* and *z* axes in the D_{2h} point group of porphine results in interchange of the subscripts 1 and 3 for B type modes. The interchange of in plane axes in the D_{4h} point group of zinc porphine has no effect on the representations but rotation of the in-plane axes by 45° interchanges the labels 1 and 2 in the B type modes.

(43) Jentzen, W.; Song, X.-Z.; Shelnutt, J. A. *J. Phys. Chem. B* **1997**, *101*, 1684−1699.

(44) Shelnutt, J. A. Unpublished crystal structures.

(45) Frydman, L.; Olivieri, A. C.; Diaz, L. E.; Frydman, B.; Morin, F. G.; Mayne, C. L.; Grant, D. M.; Adler, A. D. *J. Am. Chem. Soc.* **1988**, *110*, 336−342.

(46) Limbach, H. H.; Hennig, J.; Kendrick, R.; Yannoni, C. S. *J. Am. Chem. Soc.* **1984**, *106*, 4059−4060.

(47) Allen, F. H. *Acta Crystallogr.* **1986**, *B42*, 515−522.

(48) Steiner, T. *Angew. Chem., Int. Ed.* **2002**, *41*, 48−76.

(49) Ramirez-Cuesta, A. J. *Comput. Phys. Commun.* **2004**, *157*, 226−238.

(50) Radziszewski, J. G.; Nepras, M.; Balaji, V.; Waluk, J.; Vogel, E.; Michl, J. *J. Phys. Chem.* **1995**, *99*, 14254−14260.

(51) Plus, R.; Lutz, M. *Spectrosc. Lett.* **1974**, *7*, 73−84.

(52) Verma, A. L.; Bernstein, H. J. *Biochem. Biophys. Res. Commun.* **1974**, *57*, 255−262.

(53) Braden, D. A.; Parker, S. F.; Tomkinson, J.; Hudson, B. S. *J. Chem. Phys.* **1999**, *111*, 429−437.

(54) Hudson, B. S.; Braden, D. A.; Parker, S. F.; Prinzbach, H. *Angew. Chem. Int. Ed.* **2000**, *39*, 514−516.

(55) Braden, D. A.; Hudson, B. S. *J. Phys. Chem. A* **2000**, *104*, 982−989.

(56) Hudson, B. S. *J. Phys. Chem. A* **2001**, *105*, 3949−3960.

(57) Hamor, M. J.; Hamor, T. A.; Hoard, J. L. *J. Am. Chem. Soc.* **1964**, *86*, 6, 1938−1942.